

RSMC Tokyo – Typhoon Center

# *Technical Review*

No. 9

## Contents

N. Kohno, K. Kamakura, H. Minematsu, Y. Yorioka, K. Hisashige, E. Shimizu, Y. Sato, A. Fukunaga, Y. Taniwaki, and S. Tanijo; The Mechanism of the Storm Surges in the Seto Inland Sea Caused by Typhoon Chaba (0416).....	1
K. Kishimoto, T. Nishigaki, S. Nishimura, Y. Terasaka; Comparative Study on Organized Convective Cloud Systems detected through Early Stage Dvorak Analysis and Tropical Cyclones in Early Developing Stage in the Western North Pacific and the South Cina Sea.....	19

Japan Meteorological Agency

March 2007

## PREFACE

The RSMC Tokyo - Typhoon Center at the Japan Meteorological Agency (JMA) disseminates various tropical cyclone information products to the National Meteorological and Hydrological Services (NMHSs) concerned on a real-time basis to support their tropical cyclone forecasting and disaster preparedness and prevention activities. The Center also offers publications such as “RSMC Tropical Cyclone Best Track” and “Annual Report on Activities of the RSMC Tokyo - Typhoon Center” every year. In addition to those regular publications, the Center occasionally prepares “Technical Review” to introduce achievement of research and development on operational meteorological services for tropical cyclones.

The current issue of Technical Review contains two papers “The Mechanism of the Storm Surges in the Seto Inland Sea Caused by Typhoon Chaba (0416)” and “Comparative Study on Organized Convective Cloud Systems detected through Early Stage Dvorak Analysis and Tropical Disturbances in Early Developing Stage in the Western North Pacific and the South China Sea”. The former describes the numerical simulation of the storm surge in Japan, and the latter explains the detection of tropical disturbances in early developing stage in the Western North Pacific and the South China Sea.

The RSMC Tokyo - Typhoon Center hopes this issue will serve as useful references for the prevention of typhoon disasters.

# **The Mechanism of the Storm Surges in the Seto Inland Sea Caused by Typhoon Chaba (0416)**

**Nadao KOHNO**

*Typhoon Research Department, Meteorological Research Institute,  
1-1Nagamine, Tsukuba 305-0052, Japan*

**Kazuo KAMAKURA, Hiroaki MINEMATSU\*, Yukihiro YORIOKA,  
Kazuhisa HISASHIGE, Eichi SHIMIZU, Yuichi SATO,  
Akifumi FUKUNAGA, Yoshihiko TANIWAKI, and Shigekazu TANIJO**  
*Observation and Forecast Division, Takamatsu Local Observatory,  
1277-1 Fuki-ishi, Takamatsu 761-8071, Japan*

## **Abstract**

Typhoon Chaba in 2004 made landfall on the southeastern Kyushu and went through Chugoku (western part of Japan's Main Island) on 30 August, causing large storm surges in the Seto Inland Sea (SIS). The high tide records were broken at tide stations in Takamatsu and Uno Ports. We analyzed the tidal data and simulated this case with a numerical storm surge model.

The storm surges moved eastward along with the passage of the typhoon, and it was favorably simulated. The results revealed that the wind set-up basically played a key role in causing the large storm surges. However, the maximum storm surge (MSS) in Takamatsu did not occur when the typhoon was the nearest to the city, but about 2 hours later. Since the time of MSS approximately corresponds to the high spring tide time, the record breaking storm tide was observed there.

Moreover, we found the SIS can be divided into 6 areas according to the characteristics of sea topography and dominant wind direction by the typhoon. We also investigated the degrees of the contribution of two main factors of storm surges, i.e. inverted barometric effect and wind set-up, in each area. As a result, it turned out that the peak times of each effect were influenced by the geographical feature, as well as the wind field and the position of the typhoon, and had different characters in each area.

---

\*Present affiliation: Marine Division, Japan Meteorological Agency

*This report is basically an English-translated paper from an article in the bulletin Journal "Tenki" of Meteorological Society of Japan (MSJ).*

## 1. Introduction

Storm surges generated by typhoons have often brought large disasters in the coast of Japan. Especially, in the case of Typhoon (TY) Vera, which caused 5,098 dead or missing in 1959, most of the casualties were brought by the storm surges. The countermeasures to storm surges have developed progressively after this disaster. However, serious

storm surges still occurred. In 1991, large storm surges were generated in the western part of the Seto Inland Sea (SIS; shown in Fig. 1) by TY Mireille (Konishi, 1994; Konishi and Tsuji, 1995). However, severe disaster did not occur since the maximum storm surge (MSS) occurred just in low tide. In 1999, the storm surges by TY Bart led to serious disasters; 13 people were directly killed by storm surges in Yatsushiro Sea, and Yamaguchi-Ube airport in the Suoh-Nada (western part of the SIS) was unavailable by inundation (JMA, 2000; Kohno, 2000). The tracks of these two typhoons are almost the same and both of them generated large storm surges in Yatsushiro Sea. Recently, intense typhoons have frequently hit Japan since 2000, and serious disasters sometimes happened. In 2004, as many as ten named tropical cyclones made landfall on Japan, which is quite extraordinary since usual number is two or three. Several tropical cyclones brought disasters due to storm surges. Especially, TY Chaba generated large storm surges in the SIS, and the coincidence of MSS with the peak time of high tide caused the highest storm tide records at Takamatsu and Uno (central part of the SIS). More than 8,300 houses are inundated above the floor level only in Kagawa Prefecture, and total damages were quite enormous as 16,799 houses inundated above the floor level.

Although large storm surges sometimes occurred in the SIS due to typhoon passages as mentioned above, most cases happened in the Suoh-Nada (western part of the SIS) or the Osaka-Bay (eastern part of the SIS), and they rarely occurred in the central part of the SIS. TY Chaba is applicable to the latter case. This case is also characterized by the fact that the MSS occurred a few hours later than the time when the typhoon was

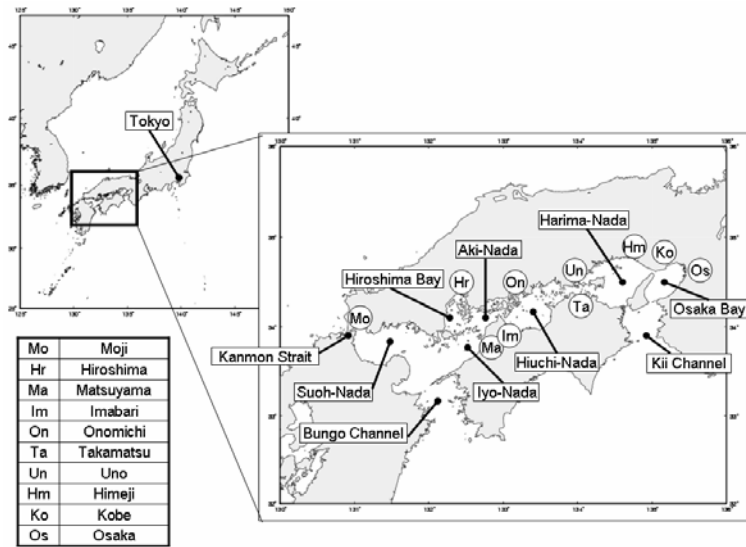


Fig. 1 Map of the western part of Japan and the Seto Inland Sea (SIS). The whole area of the Seto Inland Sea from the Suoh-Nada to the Osaka Bay is an inland sea. The points of tide stations are also shown.

nearest. Therefore we have investigated the mechanism of this storm surge with a concern to the effects of sea topography and the sequence of typhoon position, mainly based on a numerical model.

TY Chaba and storm surges in the SIS are described in section 2, and the outline of the simulation and the results are provided in section 3. Section 4 focuses on the factors that may mainly contribute to storm surges, and the conclusion is summarized in section 5.

## 2. TY Chaba (0416) and storm surges in the SIS

### 2.1 TY Chaba (0416)

A tropical depression (TD) was formed in the sea around the Caroline Islands at 06UTC (all times are expressed in UTC hereafter) on 18 August 2004. It moved slowly westward and developed into a Tropical Storm Chaba at 12UTC on 19 August. Chaba continued to move westward and was upgraded into a Typhoon at 18UTC on 21 August. Then it turned toward the northwest at the southwestern edge of sub-tropical high on 23 August. The typhoon continuously intensified during this period and developed to the strongest level as central pressure of 910hPa and the maximum wind speed of 56m/s at 18UTC on 23 August.

The typhoon kept its intensity till 18UTC on 26 August, moving to northwest and gradually weakened. The typhoon moved to west again in the sea east of the Nansei Inlands and turned to the north-northeast in the sea south of Kyushu.

The typhoon made landfall at Kushikino at about 00UTC on 30 August, with central pressure 950hPa, the maximum wind speed 41m/s, and the radius of storm wind extended to 230km east (Fig. 2). The typhoon passed through Kyushu and moved northward in the Suoh-Nada, and made landfall again at around Hohfu. As the TY Chaba approaching, Chugoku, Shikoku, northern and central part of Kinki were gradually covered by storm winds. The typhoon passed Tottori at about 12UTC with slightly

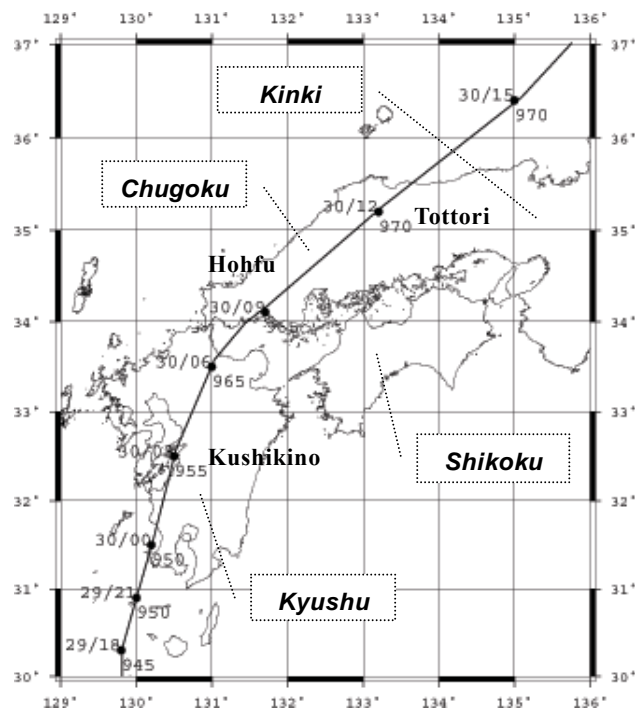


Fig. 2 Best track of TY Chaba (0416). The circles on the path indicate the positions of the typhoon every 3 hours. Days and hours (UTC) are plotted to the upper left and central pressures (hPa) to the lower right of each point.

weakened intensity (central pressure 960hPa and the maximum wind speed of 31m/s), and became to move faster in the Sea of Japan. The typhoon made landfall again at Hakodate at 03UTC on 31 August, and transformed into an extratropical cyclone in the east of Hokkaido at 06UTC.

Strong winds were observed in the areas the typhoon passed nearby. In Okayama, the maximum wind of 21.1m/s (SW) and the maximum gust of 38.5m/s (SW) were

observed at 15:20 and 12:51UTC on 30 August, respectively; those were the highest records there. The positions and intensities of TY Chaba from 06UTC on 29 to 15UTC on 30 August are listed in Table 1.

Table 1 The positions and intensities of TY Chaba from 06UTC on 29/Aug/2004 to 15UTC on 30/Aug/2004.

Date and Time(UTC)	Lat. (deg.)	Lon. (deg.)	Ps (hPa)	Max Wind (m/s)
Aug/29 0600	28.3	130.7	940	44
Aug/29 0900	28.7	130.3	940	44
Aug/29 1200	29.0	130.1	940	44
Aug/29 1500	29.3	129.9	940	41
Aug/29 1800	29.8	129.8	945	41
Aug/29 2100	30.3	129.8	945	41
Aug/30 0000	30.9	130.0	950	41
Aug/30 0300	31.5	130.2	950	41
Aug/30 0600	32.5	130.5	955	41
Aug/30 0900	33.5	131.0	965	36
Aug/30 1200	33.9	131.4	965	36
Aug/30 1500	34.1	131.7	965	36

## 2.2 Storm surges in the SIS by TY Chaba

The main storm surges in the SIS by TY Chaba occurred from 30 to 31 August. Fig. 3 shows the time series of hourly storm surges (the each storm surge is defined by deducting astronomical tide from observed sea level) observed at tide stations. The magnitudes of the MSSs are generally about 1-1.5m.

The more east the observation point is located,

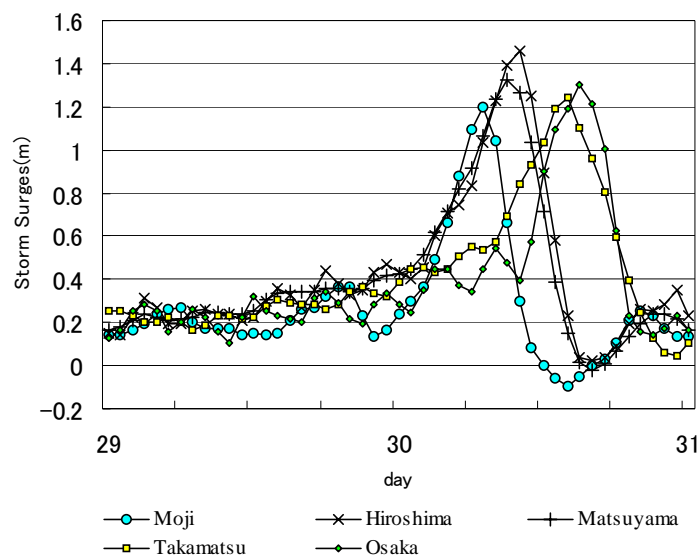


Fig. 3 Storm surges observed at several tide stations in the Seto Inland Sea.

the later the MSS was observed. (Table 2). For example, in the western part of the SIS, the MSS of 1.33m in Moji was observed at 06:36. The MSSs in Hiroshima and Matsuyama occurred at 09:35 (1.49m) and 08:49 (1.40m), respectively. MSSs in Takamatsu and Uno were observed after 13UTC, 4 hours later than that in Matsuyama. The MSS of 1.33m was observed at 13:23 in Takamatsu, and 1.37m at 13:16 in Uno. In Kobe and Osaka, that are in the eastern part of the SIS, the MSSs were observed just before 15UTC: 1.34m at 14:42 in Kobe and 1.32m at 14:30 in Osaka.

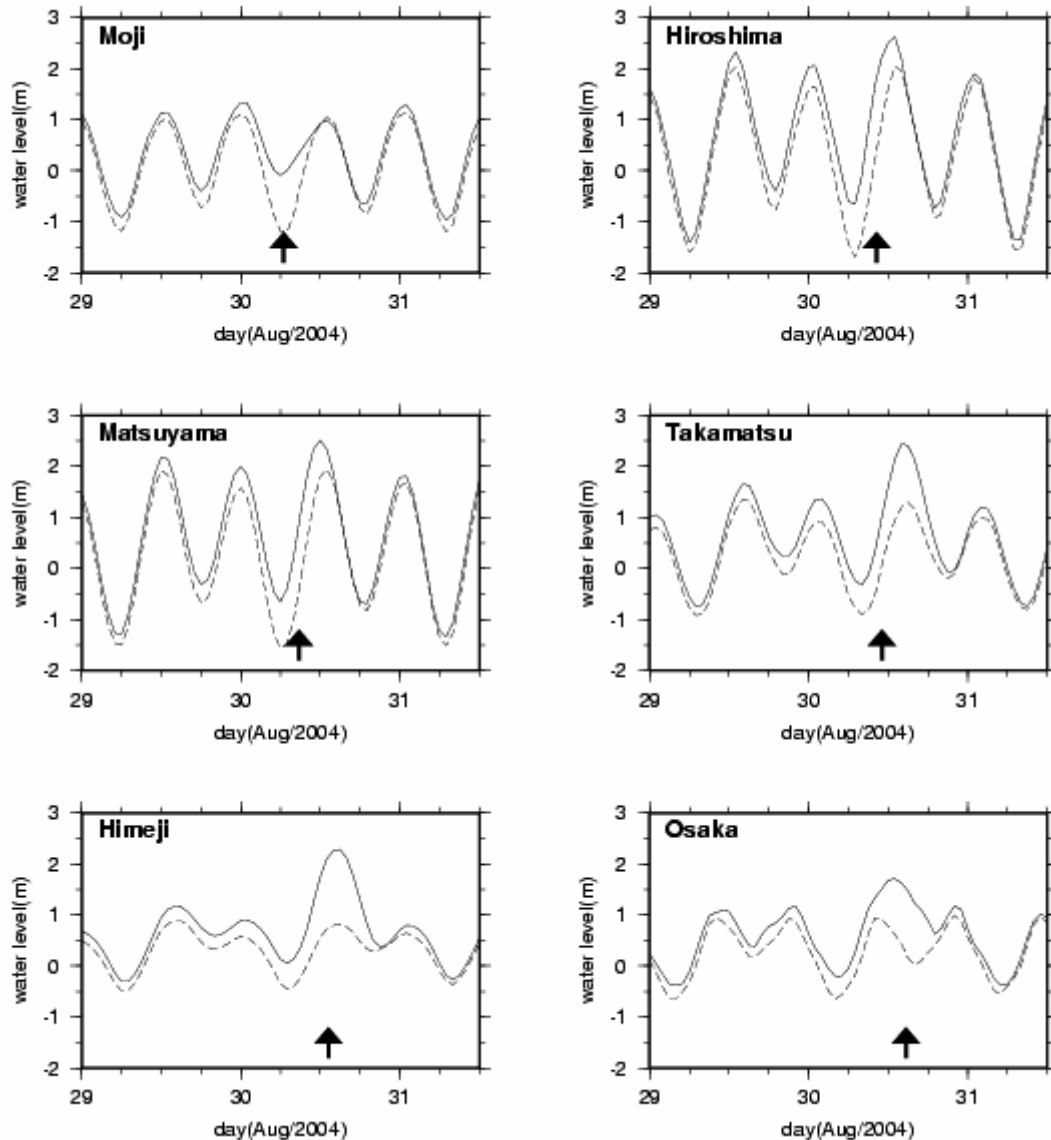


Fig. 4 The observed sea levels at several tide stations in the Seto Inland Sea. The observed sea levels are indicated by a solid line; the broken line represents the astronomical tide. The arrows show the time of the minimum surface pressure.

Fig. 4 shows the water levels at several tide stations. The magnitudes of the storm surges are not so different among these points, but the magnitudes of the storm tides are different each other because the timing of the astronomical tides are different

each other. Since the time of MSSs were the same as that of low tide in Moji, storm tides did not become so high; the maximum tides were observed about 6 hours earlier than the time of MSS (around 00:30), this was mostly contributed by high tide, not the storm surge. The maximum storm tides of 2.58m (Matsuyama) and

Table 2 The maximum storm surges (MSS), the minimum sea level pressures (MSLP) and the difference of time.

Tide station	MSS (m) and time (UTC)	MSLP (hPa) and time(UTC)	difference of time (min.)
Moji	1.33 (06:36)	969.5 (06:30)	6
Hiroshima	1.49 (09:35)	972.1 (10:16)	-41
Matsuyama	1.40 (08:49)	972.8 (08:49)	—
Uno	1.37 (13:16)	978.1 (10:48)	148
Takamatsu	1.33 (13:23)	978.1 (11:01)	132
Himeji	1.57 (14:50)	982.7 (13:13)	97
Kobe	1.34 (14:42)	987.5 (14:05)	37
Osaka	1.32 (14:30)	988.1 (13:42)	48

2.69m (Hiroshima) were observed at 11:56 and 12:56 respectively, 2-3 hours earlier than the high tides. The maximum storm tide there results from combination of storm surge and astronomical tide. The maximum storm tides were observed in Takamatsu and Uno at 13:42 and 13:47, respectively, only 30 minutes later than MSS. Moreover, since it was period of spring tide, water levels at high water were higher than usual. This also led to the highest record of maximum tides as 2.46m (Takamatsu) and 2.54m (Uno). This extraordinary high storm tide caused enormous disasters, and more than 12,000 houses were flooded to over floor level in these coastal areas. The maximum storm tides were observed at 12:24 in both Kobe and Osaka to the east of Takamatsu, which was about 2 hours earlier than the time of MSSs.

In order to investigate the relation of storm surges to the relative position of typhoon, the time of MSS and the time when the minimum sea level pressure (MSLP) was observed, which corresponds to the time when the typhoon mostly approached, are listed in Table 2. The easterly wind was predominant in the western part of the SIS as the typhoon was approaching, and the sea level became higher from early stage in the Suoh-Nada. Around the Suoh-Nada area, the times of MSSs were almost the same as the time of the MSLP, since the typhoon passed through the Suoh-Nada. For example, in Moji, the time of MSS (1.33m) was only 6 minutes later than MSLP time. After the typhoon passed and made landfall at Chugoku region, the predominant wind turned to westerly in the wake of typhoon, and large storm surge area shifted to the eastern part of the SIS gradually. The MSS was observed at almost the same time of MSLP in Matsuyama, but was 41 minutes earlier in Hiroshima. At the points to the east of Matsuyama, the MSSs were observed later than the time of the MSLP.

It is notable that the times of MSS in Takamatsu and Uno were more than 2 hours

later than the times of the MSLPs, but in Himeji and Osaka, located in further east of Uno, the difference of times between MSS and MSLP became smaller again. This indicates that the storm surge area did not move monotonously to east while the typhoon was simply leaving northward.

### 3. Numerical simulation with storm surge model

#### 3.1 Outline of the storm surge model and numerical methods

The basic equations of the storm surge model are momentum flux and continuity of water mass under the rotating field with gravitational acceleration.

$$\frac{\partial Du}{\partial t} + \frac{\partial Du^2}{\partial x} + \frac{\partial Du v}{\partial y} = -\frac{g}{\rho_w} D \frac{\partial(\zeta - \zeta_0)}{\partial x} - \frac{1}{\rho_w} (\tau_{ax} - \tau_{bx}) + f D v \quad (3.1)$$

$$\frac{\partial Dv}{\partial t} + \frac{\partial Du v}{\partial x} + \frac{\partial Dv^2}{\partial y} = -\frac{g}{\rho_w} D \frac{\partial(\zeta - \zeta_0)}{\partial y} - \frac{1}{\rho_w} (\tau_{ay} - \tau_{by}) - f D u$$

$$\frac{\partial \zeta}{\partial t} + \frac{\partial Du}{\partial x} + \frac{\partial Dv}{\partial y} = 0 \quad (3.2)$$

where  $(x, y)$  shows horizontal direction,  $\mathbf{U} = (u, v)$  current components,  $\zeta$  height deviation,  $\zeta_0$  balance level with surface pressure,  $\rho_w$  sea water density,  $f$  Coriolis parameter, and  $g$  gravitational acceleration.  $D$  shows the local water depth.

The surface stress  $\boldsymbol{\tau}_a = (\tau_{ax}, \tau_{ay})$  by winds and the bottom stress  $\boldsymbol{\tau}_b = (\tau_{bx}, \tau_{by})$  are estimated with surface winds  $\mathbf{V} = (v_x, v_y)$  and  $\mathbf{U}$  as follows:

$$\begin{aligned} \boldsymbol{\tau}_a &= -\rho_a C_{da} |\mathbf{V}| (v_x, v_y) \\ \boldsymbol{\tau}_b &= -\rho_w C_{db} |\mathbf{U}| (u, v) \end{aligned} \quad (3.3)$$

where  $\rho_a$  is air density,  $C_{da}$  and  $C_{db}$  indicate the drag coefficients and their values are defined empirically as

$$\begin{aligned} C_{da} &= 3.2 \times 10^{-3} \\ C_{db} &= 2.5 \times 10^{-3} \end{aligned} \quad (3.4)$$

The coastal boundary was assumed to be a ‘‘rigid wall’’, and no inundation or dry-up were considered. The boundary of open sea was assumed to maintain a static balance with the surface pressure, and a deviation from the statically balanced level makes inflow or outflow current as a gravitational wave.

The surface pressure field  $P_s$  is defined by the formula of Fujita (1952), using the parameters of the 3 hourly JMA best track data,

$$P_s(r) = P_\infty - \frac{P_\infty - P_c}{\sqrt{1 + (r/r_0)^2}} \quad (3.5)$$

where  $P_c$  is the central pressure,  $P_\infty$  the environmental pressure and assumed to be

constant as 1012hPa. The parameter  $r_0$ , which indicates typhoon size, is determined from substituting the radius of 1000hPa in a weather chart to (3.5).

The gradient wind derived from this profile gives the symmetrical surface wind, and the surface wind is defined to be asymmetrical by adding a typhoon moving speed to this gradient wind with a constant inflow angle of

30 degrees. The surface stress is obtained by substituting this surface wind to  $\mathbf{V}$  in (3.3).

The computational area was set from 32°N to 35°N and from 130°E to 136°E, which covers the whole SIS, and the horizontal grid resolution was 1 minute (corresponds to a physical distance of 1.85km in latitude and 1.55km in longitude). The domain and sea topography used in the calculation are shown in Fig. 5. The calculation time step was 2 seconds, which completely satisfies the CFL condition since even the largest water depth does not exceed 1,000m. This grid resolution was not enough to express the Kanmon Strait, and sea water could not pass through. However, the gross characteristic of the storm surge in the SIS is supposed to be expressed adequately since the amount of sea water flow via channels such as the Bungo Channel, which is well represented, is far larger than that of the Kanmon Strait.

We conducted the simulation from the static initial state. Considering the earlier part being spent for spin up, we started the calculation from 00UTC on 29 August, two days before the typhoon hit the SIS.

### 3.2 Simulation results

Fig. 6 (a) shows the simulated storm surge distributions as well as the surface winds used in the calculations. The observation of winds is not so dense in this area, especially in the sea, for intensive comparison. Therefore, the surface winds of the hourly objective analysis, which is based on the operational Meso-Scale Model (MSM) prediction as a first guess and modified with the wind profiler observation, and shown in Fig. 6 (b), will be used for discussion in the next section. Although the hourly objective analysis does not represent the true atmosphere sufficiently, we assume that it is more realistic than the wind field derived from eq. (3.5).

Storm surges are little detected in the whole area before the typhoon reached Kyushu and a gale wind started. In the Suoh-Nada, large storm surge area is generated by strong easterly wind ahead of the approaching typhoon (06UTC on 30 August). As the

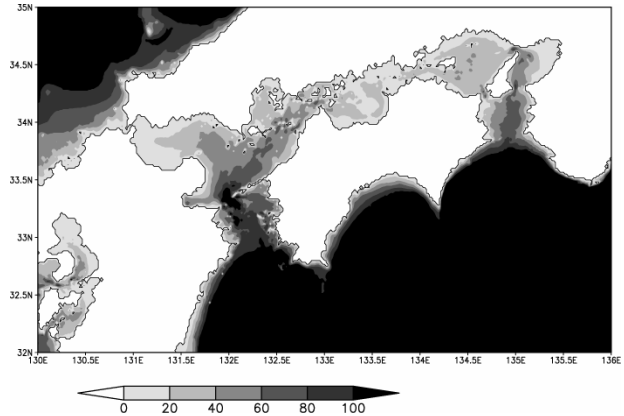


Fig. 5 The computational domain and water depth (m).

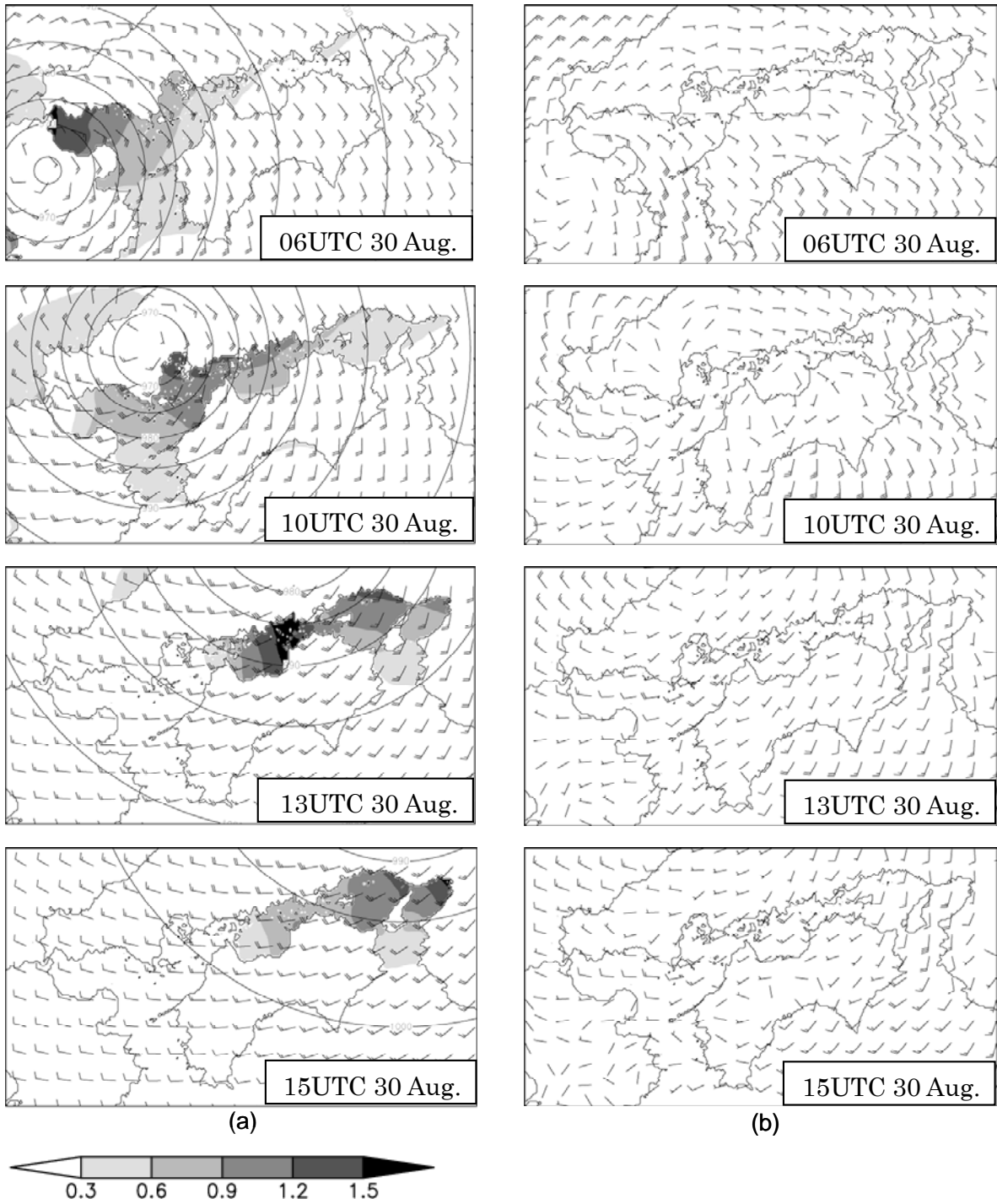


Fig. 6 Horizontal distribution of (a) the simulated storm surge and the model wind, and (b) the surface wind of the hourly objective analyses. The shades indicate simulated storm surges (m), and the contours in the left column show the model surface pressure. The barbs in both columns show the winds (long fletching is 10m/s, and short 5m/s).

typhoon had passed the Suoh-Nada and moved northeastward, the wind turned to westerly, which led the large storm surge area to move eastward (10UTC). Around 13UTC, although the typhoon had already moved away northward, a large storm surge is notable in the central sea to the west of a narrow straight (just where Takamatsu and Uno

exist). After that, although the typhoon continued to leave further, westerly wind continued to blow, and storm surge shifted eastward, to the Osaka Bay around 15UTC on 30 August.

The calculated MSSs at several points are listed in Table 3, and Fig. 7 shows the time series at Takamatsu: Observed and calculated storm surges, observed sea level pressures as well as those used in the model. According to Tables 2 and 3, all the calculated MSSs are favorably compared with observation and every error are within 0.30m. However, there are almost 1 hour differences in peak time at some

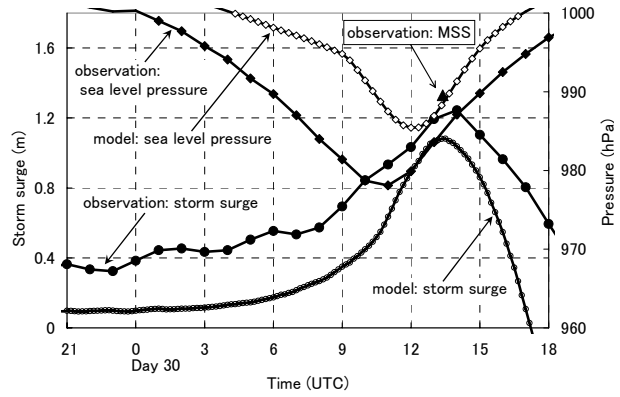


Fig. 7 The time series at Takamatsu

points. This may mainly come from the error of meteorological data input, e.g. assumed pressure field given with eq. (3.5), since the time of minimum surface pressure given to the model is different from that of observation as shown in Fig. 7. The difference of pressure fields may also lead to the error of wind fields, but the wind fields in the time of MSS at Takamatsu was preferably estimated as shown in Fig. 6.

Table 3 The results of three calculations. Simulated magnitudes of the maximum storm surges (MSS), given MSLP with the occurrence time in parenthesis. Contribution ratio of the wind set-up in the MSS, CR, defined as the MSS in II divided by that in I is also listed.

Tide station	MSS(m) in I	MSLP (hPa)	MSS (m) in II	MSS (m) in III	CR
Moji	1.61 (05:40)	969 (07:20)	1.35 (05:20)	0.52 (08:40)	84%
Hiroshima	1.44 (10:10)	969 (10:20)	1.01 (08:50)	0.70 (11:10)	66%
Matsuyama	1.15 (10:30)	978 (10:00)	0.70 (10:20)	0.50 (11:00)	60%
Uno	1.19 (12:40)	983 (12:00)	0.89 (12:20)	0.49 (14:00)	74%
Takamatsu	1.08 (13:30)	985 (12:00)	0.76 (12:50)	0.47 (14:20)	69%
Himeji	1.47 (13:50)	985 (13:20)	1.16 (13:30)	0.46 (15:20)	78%
Kobe	1.40 (14:30)	990 (13:40)	1.11 (14:20)	0.36 (15:50)	79%
Osaka	1.62 (14:40)	991 (14:00)	1.35 (14:30)	0.37 (15:50)	82%

#### 4. Discussion

Generally speaking, storm surges are mainly caused by two factors: the inverted

barometric effect and the wind set-up (e.g. Miyazaki, 2003). Both of the effects are easily estimated to some extent by assuming the static balance. In addition, it is known that, as Arakawa and Yoshitake (1935) pointed out, the dynamical effects such as resonance of the moving speed of meteorological disturbance and surface water movement as ocean long wave may cause large storm surges.

Since the numerical simulation model enables to include such dynamical effects without any simplification of topography, we will be able to proceed to discuss how the two main effects functioned in the simulation.

To detect these effects, we carried out two additional simulations: One is that only the wind effects are considered by setting the pressure force in the second term on the right side of (3.1) to  $\zeta_\theta = 0$  (hereafter we refer to as the “wind calculation”), and the other is that only the pressure effects are considered by setting the wind stress in the third term on the right side of (3.1) to  $\tau_a$  to 0 (hereafter we refer to as the “pressure calculation”). We represent I as the control calculation, II as the “wind calculation”, and III as the “pressure calculation”. The MSSs by every calculation are listed in Table 3.

#### 4.1 The inverted barometric effect

The results of III show that all the MSSs appeared after the time when the typhoon was nearest; especially the delay became large in the Hiuchi-Nada and the Osaka Bay, that is, Uno, Takamatsu, Himeji, Kobe and Osaka. The reason is supposed that the eastward movement of water piled up in the western part of the SIS was prevented at the narrow part of the east channel surrounded by the ellipse in Fig. 8 (a). In order to verify this hypothesis, a calculation with an experimental topography as shown in Fig. 8 (b) was conducted. (The channel part is enlarged and changed to the sea with 20m depth.) The result showed that the times of the MSS in the west of the Iyo-Nada were hardly changed.

On the one hand, those in the east of the Iyo-Nada became earlier and the delay of time decreased (not shown). For example, the time became earlier about 20 minutes in

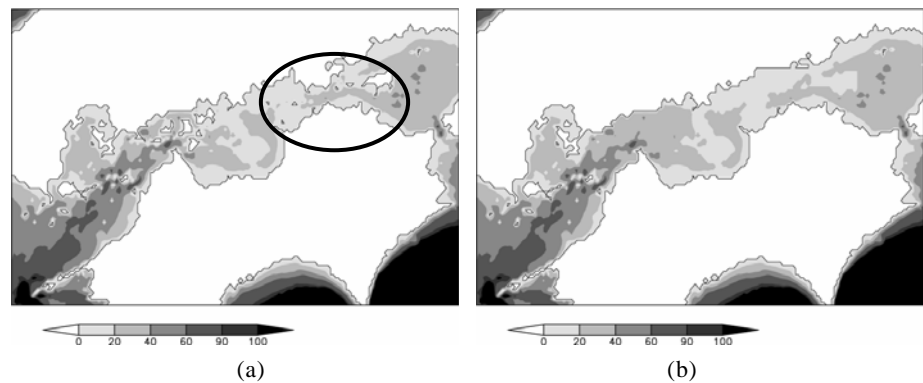


Fig. 8 (a) The original topography, (b) The test one where the east channel is extended.

Takamatsu and Uno, and about 40 minutes in the Hiuchi-Nada at most.

If the static balance ( $\cong 1\text{cm/hPa}$ ) is assumed, the amount of surge by inverted

barometric effect can be estimated to be 30 - 40cm from the minimum surface pressure, that are generally 10cm smaller than the MSSs of III. The reason of this difference may be that sea water was preferably piled up, due to the inertia of sea water and the narrow strait as an “obstacle”. Therefore, the dynamical inverted barometric effect with an influence of sea topography is likely to give larger MSS than only static one would give in this area.

#### 4.2 The wind set-up

The wind set-up is the major effect of the large storm surges. The “contribution ratio” of the wind set-up in the MSS defined as the MSS in II divided by that in I, (hereafter CR) was calculated in several tide station points. CR shows high value in every point as 70 - 80% (except Matsuyama of 60%). This indicates that the wind change along with a moving typhoon had an important role.

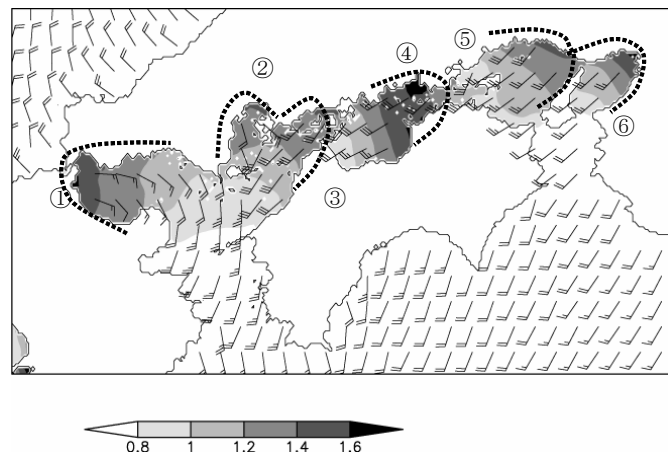


Fig. 9 The maximum storm surges (m) calculated in every grid and wind at same time

#### 4.3 The characteristic differences among local seas

Fig. 9 shows the amplitudes of the MSS at every grid point and surface wind corresponding to the occurrence time of the calculation I. This distribution reveals several clusters of large storm surge area and wind direction. The storm surge in each area behaves as if the area is a bay, where large storm surge is generated in the most inner part by an inflow wind. By considering this characteristic, we divide the SIS into 6 local seas as shown in Fig. 9.

- ① the sea opening to east with the Kanmon Strait as a wall (the Suoh-Nada)
- ② the sea opening to south with the north coast of Hiroshima (the Hiroshima Bay)
- ③ the sea opening to southwest, closed by islands around Imabari (the Iyo-Nada and the Aki-Nada)
- ④ the sea opening to west, closed by the narrow channels (the Hiuchi-Nada)
- ⑤ the sea opening to south with the north coast of Himeji (the Harima-Nada)
- ⑥ the sea opening to south with the north coast of Osaka (the Osaka Bay)

Fig. 10 depicts the time series of the model sea level pressure and the storm

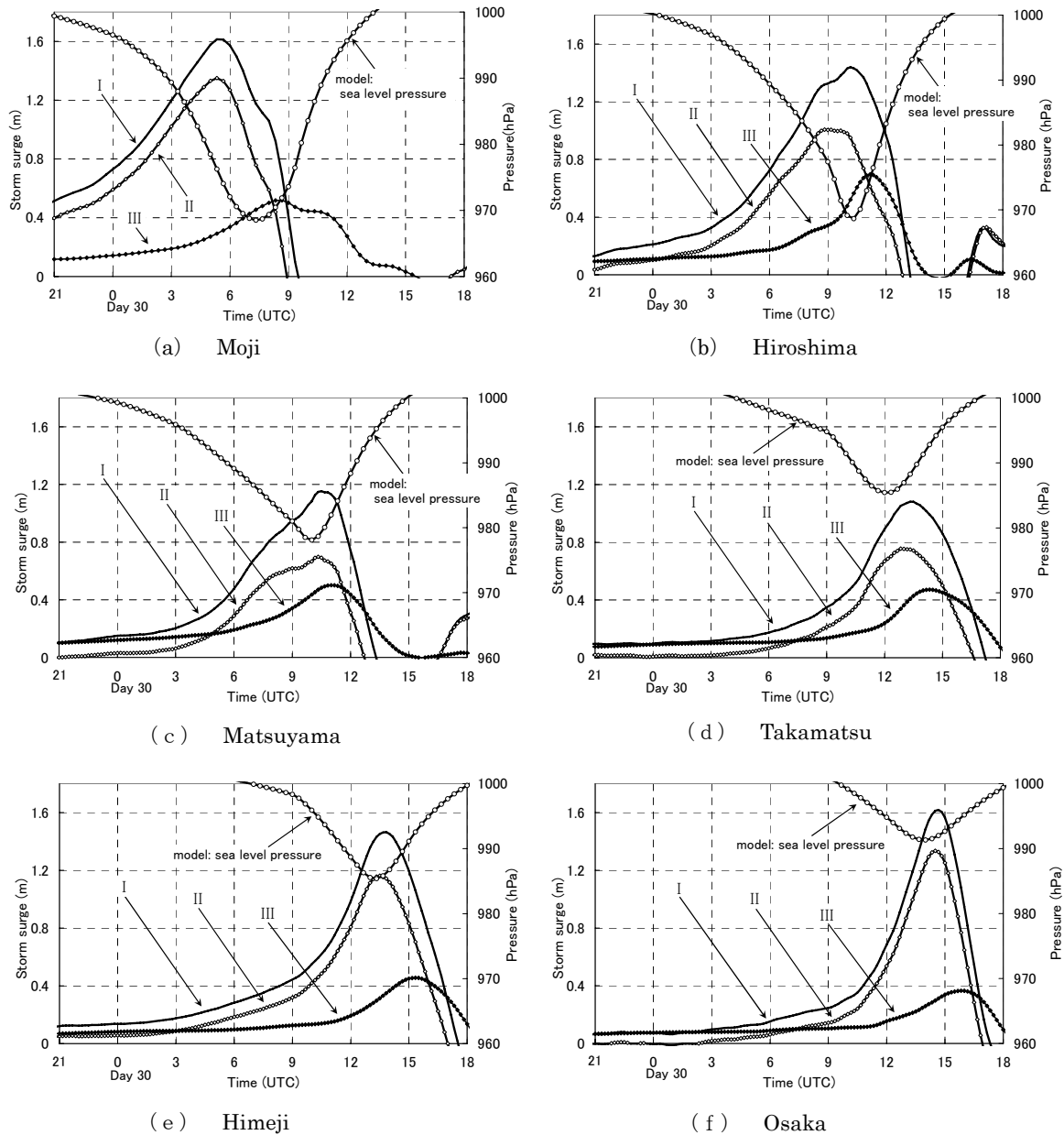


Fig. 10 The time series of calculation results in each area. The surface pressure (hPa) and calculated storm surges (m) by the cases of I, II, and III.

surges in calculations I, II, and III at a point of each sea. We describe on the characteristic points in every sea.

① the Suoh-Nada (tide station: Moji)

At Moji, the MSS of 1.33m was observed at 06:36 (Table 2), while 1.61m at 05:40 in calculation (Fig. 10a and Table 3). According to the hourly objective analyses in Fig. 6, easterly wind of 15m/s blow at the time of peak surge, which agrees with the model wind. The storm surge was generated mainly by this easterly wind. Since the effect of wind set-up can be estimated as follows if we assume a static balance:

$$\Delta z \propto \frac{\tau}{\rho_w g D} \cdot L \approx \frac{\rho_a C_{da} U^2}{\rho_w g D} \cdot L.$$

The surge anomaly  $\Delta z$  is proportional to stress  $\tau$ , horizontal scale  $L$ , and the inverse of water depth  $D$ . The water depth in the Suoh-Nada is shallower than other seas as shown in Fig. 5, which lead to the largest CR of 84%. In addition, the southerly wind at the Bungo Channel induces large amount of sea water inflow to the Suoh-Nada. An additional calculation with the closed Bungo Channel reveals that the MSSs decreased by 0.13m at Moji and 0.30m at Tokuyama (eastern part of the Suoh-Nada) without inflow through the Bungo Channel.

Therefore, the storm surge in the Suoh-Nada is explained mainly by the wind set-up of easterly wind ahead of the typhoon, and the sea water provided via the Bungo Channel enlarged it.

#### ② the Hiroshima Bay (Hiroshima)

At Hiroshima, the MSS of 1.49m was observed at 09:35 (Fig. 3 and Table 2), which is favorably simulated by the calculation of 1.44m at 10:10 (Fig. 10b and Table 3). The wind of hourly objective analyses shows 15 - 25m/s (S - SSW) during 09 to 10UTC, when the MSS occurred. The wind given to the model is almost the same, though the wind direction is rather S to SW. The storm surges in the Hiroshima Bay are explained by the wind set-up of this southerly wind. The wind turned to SW from SE as the typhoon moved northeastward, but it kept southerly direction, which was preferable for large storm surge.

#### ③ the Iyo-Nada and the Aki-Nada (Matsuyama)

At Matsuyama, the MSS of 1.40m was observed at 08:49 (Fig. 3 and Table 2), while the MSS of 1.15m is calculated later at 10:30 (Fig. 10c and Table 3). According to the hourly objective analyses, the wind at the Iyo-Nada was about 15m/s (SW - SSW) around 09UTC, but the direction of model wind was southerly and the MSS occurred after the wind turned to SW. The fact that the time of the MSS coincides with the SW wind suggests that the MSS occurs when SW wind is predominant, and the coast around Imabari works as if it is a wall.

CR is the lowest (60%) among 8 tide station points because of its deep water depth. The contribution of the inverted barometric effect is relatively higher at Matsuyama than at other areas.

#### ④ the Hiuchi-Nada (Takamatsu)

At Takamatsu, the MSS of 1.33m was observed at 13:23 (Fig. 3 and Table 2),

which is favorably simulated by the calculation of 1.08m at 13:30 (Fig. 10d and Table 3). The result at Uno was also reasonable. The wind during 13 to 14UTC, when the MSSs were observed at Takamatsu and Uno in the Hiuchi-Nada, was about 20m/s (WSW-SW) by both of the hourly objective analyses and wind given by the model, which caused similar storm surges by the wind set-up of westerly wind, and the peak was generated in the part to the west of the narrow channel between Uno and Takamatsu. The maximum of the inverted barometric effect appeared about 2 hours later than the minimum surface pressure. The reason of the delay is that flow of the sea water was reduced by the narrow east edge of the Aki-Nada.

The dominant wind direction is south while Takamatsu is open northward. Therefore, it is not reasonable to explain this storm surge simply by the local wind set-up. There may be possibility of any seiche being excited by own topography scale, but no such oscillation is detected. We consider that the storm surges in the Hiuchi-Nada was caused mainly by the accumulation of sea water, prevented from moving eastward at the narrow channel between Takamatsu and Uno.

According to a simulation with the channel between Imabari and Onomich being closed to reduce the inflow from the Aki-Nada, storm surges occurred but the maximum value decreased by 0.3 to 0.5m. This supports the speculation that the sea water from the Aki-Nada contributed to the storm surge in the Hiuchi-Nada.

#### ⑤ the Harima-Nada (Himeji)

At Himeji, the MSS of 1.57m was observed at 14:50 (Fig. 3 and Table 2), while the calculation was 1.47m at 13:50 (Fig. 10e and Table 3). The CR is as high as 78% and the wind set-up by SW wind generated the storm surges in the Harima-Nada. Since the model wind agrees well with the wind of hourly objective analyses of 15-30m/s (S-SSW), and this sea opens southward and southwestward equally, the simulated result agrees well with the observation. Although the east Harima-Nada is connected to the Kii Channel via the Naruto Strait, the inflow of sea water through the narrow strait is supposed to be negligible.

#### ⑥ the Osaka Bay (Osaka and Kobe)

At Osaka, the MSS of 1.32m was observed at 14:30 (Fig. 3 and Table 2), and 1.34m was observed at 14:42 at Kobe (Table 2). The calculation was 1.62m at 14:40 at Osaka (Fig. 10f and Table 3), 1.40m at 14:30 at Kobe (Table 3). The wind direction given by the model is different from that of the hourly objective analyses. The wind given by the model was southwesterly, and the MSS at Osaka was larger than that at Kobe due to its longer fetch. On the contrary, the wind of hourly objective analyses was southerly, which gives the same fetch both to Osaka and Kobe, and the MSSs were the same

magnitude. Since the water depth in the Osaka Bay is shallow, CR at Osaka and Kobe is as high as 79 – 82%.

Therefore the storm surge in the Osaka Bay as well as the Harima-Nada was mainly caused by the wind set-up of S – SW winds.

#### **4.4 The further factors which may cause errors between calculation and observation**

The calculation results show good agreement with observation, but there are still different points.

At first, the simulated amplitude of MSS at Moji is larger by 30cm than observed. This may be mainly because that Moji is located rather in the Kanmon Strait, not in the Suoh-Nada. The storm surge at Moji should be decreased by the water flow in this narrow Strait. A test calculation with exaggerated expression of wider strait led to an underestimation of storm surge, but storm surges calculated with closed strait showed much similar tendency to observation in quality. This suggests that the storm surge at Moji could be regarded as the phenomena at the western edge of the Suoh-Nada.

It should be also noted that the wind given by the model was about 10m/s larger than the hourly objective analyses, and the wind direction given by the model and that by the hourly objective analysis were, respectively, easterly and northerly. This might also lead to the larger storm surge by the model. This problem is also raised in the Osaka Bay as mentioned in the previous subsection.

Next, the MSS in Hiroshima occurred about 40 minutes later than that in Matsuyama, although Matsuyama is located to the east of Hiroshima. It seems to be mainly because Hiroshima is located in the most inner part of the bay. It took much time for waters to reach Hiroshima since Bohyo Islands are located in the SW of the Hiroshima Bay. Sea water seems to be prevented from moving northward by these islands.

The predominant wind direction was also different in the Kii Channel; the wind direction in the hourly analyses was bent to south by the topography. This may also lead to the errors in the Osaka Bay.

All of these problems essentially come from the wind fields, which are deduced from the ideal profiles of pressure approximated with eq. (3.5). The real structure of a typhoon is so complicated and the wind in the core area is far from being uniquely determined. Moreover, the wind is modulated by the topography, and the wind distribution is usually not simple. The “errors” of wind fields surely bring error in storm surges estimation. Therefore, a storm surge simulation with more realistic winds should be developed.

## **5. Conclusion**

The mechanism of the storm surges in the SIS caused by TY Chaba in 2004 was investigated and our conclusions are summarized as follows:

- (1) The storm surges by TY Chaba are mainly caused by the wind set-up effect.
- (2) The SIS is divided into six areas in terms of the characteristics of the storm surge caused by TY Chaba. Each area is characterized by the preferred wind direction, relative importance of wind set-up effect and piling up of the sea water.

a. The Suoh-Nada

The wind set-up is extremely predominant due to its shallow water depth. The inflow of sea water from the Bungo Chanel also influences on the storm surges.

b. The Hiroshima Bay

Since the typhoon passed nearby and the duration of southerly wind was long, the wind set-up continued longer than other areas.

c. The Iyo-Nada

The wind set-up is not so predominant due to deep water. However, the coincidence of the time of the maximum inverted barometric effect and that of the wind set-up causes large storm surge.

d. The Hiuchi-Nada

The peak of inverted barometric effect appeared after the typhoon approached to the nearest because of the pile up of the sea water in the Aki-Nada. The coincidence of the time of the maximum inverted barometric effect and that of the wind set-up causes large storm surge similar to the Iyo-Nada.

e. The Harima-Nada and the Osaka Bay

The wind set-up functioned well since the sea opens to south and southwest and water depth is shallow.

- (3) The time of the MSS was different among the areas. The time is almost the same as the time when the typhoon was nearest in the western part, although it delayed in the eastern part, especially the delay of time in the Hiuchi-Nada was over 2 hours. This indicates that storm surges in the SIS have good chances to occur after a typhoon passing away by the influence of sea topography. The timing of MSS was also influenced by the change of wind directions along with the typhoon movement.

Since it is rather common for a typhoon to pass along the same course as TY Chaba, that made landfall in Kyushu and passed into the Sea of Japan, it is likely that similar storm surges also happen frequently. Therefore we will research other storm surge cases to detect the mechanism as well.

## **Acknowledgements**

This report summarized the results of the cooperative research of “Numerical study

of the storm surges in the SIS caused by Typhoon Chaba in 2004” carried out by Meteorological Research Institute (MRI) and Takamatsu Local Observatory in 2004. It partly contains the results of the research project of “Study of processes of structural change of typhoons made landfall and the occurrence of strong wind, heavy rains, storm surge and high wave” in MRI. The authors would like to express their sincere gratitude to Dr. Ohno, the Director of the Takamatsu Local Observatory, for his helpful comments and continuous encouragement.

Some of data used in this research are collected in the “Urgent research about typhoons made landfall on Japan in 2004” of MRI, and the authors also show thanks to the organizations concerned for providing their data.

## References

- Arakawa, H. and M. Yoshitake, 1935 : Report on the ‘Muroto Taifu’ in 1934, 347-361. (in Japanese)
- Fujita, T., 1952 : Pressure distribution within typhoon, Geophysical Magazine, 23, 437-451.
- Japan Meteorological Agency, 2007, Outline of the Operational Numerical Weather Prediction at the Japan Meteorological Agency, 194pp, Available at "<http://www.jma.go.jp/jma/jma-eng/jma-center/nwp/outline-nwp/index.htm>"
- JMA, 2000 : Report on the storm surges by Typhoon Bart (No.9918) in September 1999, Japan, Technical Report of the Japan meteorological Agency, 122, 168pp. (in Japanese)
- Konishi, T., 1995 : Storm surges in the western part of the Inland Sea, caused by Typhoon 9119 –analyses of tidal records, documents on flooding and field inspection-, Umi to Sora (SEA AND SKY), 70, 171-188. (in Japanese)
- Konishi, T. and Y. Tsuji, 1995 : Analyses of Storm Surges in the western part of the Seto Inland Sea of Japan caused by Typhoon 9119, Continental Shelf Res., 15, 1795-1823.
- Kohno, N., 2000 : The mechanism of storm surges caused by TY BART(9918) in 1999, KAIYO MONTHLY, 32, 763-770. (in Japanese)
- Miyazaki, M., 2003 : Research on Storm surges. The Examples and Mechanism, Seizando Press, 61-68. (in Japanese)

# Comparative Study on Organized Convective Cloud Systems detected through Early Stage Dvorak Analysis and Tropical Cyclones in Early Developing Stage in the Western North Pacific and the South China Sea

**Kenji KISHIMOTO, Tsuguhito NISHIGAKI**

*National Typhoon Center, Japan Meteorological Agency*

**Shuji NISHIMURA, Yoshiyuki TERASAKA**

*Meteorological Satellite Center, Japan Meteorological Agency*

## Abstract

The Japan Meteorological Agency (JMA) has been operating the satellite image analysis for tropical cyclones (TCs) in early developing stage such as tropical depressions (TDs) since 2001 to detect them and diagnose their possibility to develop into tropical storms (TSs). The analysis, which is based on Dvorak (1984), is referred to the early stage Dvorak analysis (EDA) in this report. Comparing organized convective cloud systems (OCCSs) detected through EDA with TCs on weather charts from 2002 to 2006, the detected OCCSs can be acknowledged as follows:

- TDs usually have an OCCS detected through EDA, while low pressure areas (LPAs) do not.
- OCCSs determined as the T-number of less than 1.0 have considerable possibility (about 50%) to develop into TDs with the 10-minute maximum sustained wind (MSW) of less than Beaufort Force 7. On the other hand, few (about 5%) OCCSs develop into TDs with MSW of less than Force 7 before the first detection of OCCSs.
- OCCSs determined as the T-number of 1.0 (T1.0) have very high possibility (about 80%) to develop into TDs with MSW of Force 7 and high possibility (about 60%) to develop into TSs. Before or at the first T1.0 determination, many (about 75%) of them develop into TDs of with MSW of less than Force 7.
- OCCSs determined as T1.5 have very high possibility (about 80%) to develop into TSs. Before or at the first T1.5 determination, many (about 80%) of them develop into TDs with MSW of Force 7.
- Most (near 100%) of OCCSs determined as T2.0 develop into TSs.

## 1. Introduction

Geostationary meteorological satellite imagery is one of the most important tools

for analyzing tropical cyclones (TC)<sup>1</sup> in the tropical ocean which has few synoptic surface observations. Since 2001, the satellite image analysis has been operated for TCs in early developing stage by the Meteorological Satellite Center (MSC)<sup>2</sup> of the Japan Meteorological Agency (JMA), in addition to the satellite image analysis for ones developed to approximate tropical storm (TS) intensity or higher which has been conducted for more than 20 years. Both analyses are based on Dvorak (1984). In this report, the former one is referred to as the early stage Dvorak analysis (EDA), while the latter one is referred to as the Dvorak analysis.

The results of EDA are used for the JMA headquarters (JMAHQ) not only to detect TCs in weather map analysis but also to diagnose their possibility to develop to TS intensity. They have been archived since 1999 when MSC started the experimental operations of EDA. So far, several studies using these archives have been already conducted. Ueno (2002) and Terasaka et al. (2007) verified the diagnosis of the development into TSs using the 2-year data from 2000 to 2001, and the 6-year data from 2000 to 2005, respectively. In addition, Bessho et al. (2006) investigated the frequency of occurrence, geographical distribution, and duration of organized convective cloud system (OCCSs)<sup>3</sup> using the 4-year data from 2002 to 2005. The main purpose of these studies was to verify the diagnosis of the development into TSs. Therefore, this study mainly focuses on the verification of EDA with respect to the detection of TCs in early developing stage by comparing OCCSs detected through EDA with TCs on weather charts.

Hereinafter, the TC analysis of JMAHQ and EDA of MSC are introduced in Section 2. Then, the verifications and their discussions are described in Section 3, and finally summarized in Section 4.

## **2. TC analysis of JMA**

### **2.1 TC analysis of JMAHQ**

JMAHQ analyze TCs in the western North Pacific and its adjacent seas including the South China Sea to issue weather information for ships such as marine warning and Asia-Pacific surface analysis (ASAS). At the same time, as the Regional Specialized

---

1 In this report, "tropical cyclone (TC)" is used as a generic term that includes "low pressure area (LPA)", "tropical depression (TD)", "tropical storm (TS)", "severe tropical storm (STS)" and "typhoon (TY)". LPA, TD, TS, STS and TY are defined in WMO (2005).

2 The operation of both analyses is going to be transferred from MSC to the JMA headquarters in 2007.

3 In this report, an "organized convective cloud system (OCCS)" is defined as a convective cloud system with a cloud system center (CSC). "CSC" is explained in Section 2.2. A convective cloud system is seen as a group of convective cloud areas including convective cloud bands and lines in satellite imagery.

Meteorological Center (RSMC) with specialized activities in analysis and forecasting of TCs in the above area within the framework of WMO, JMAHQ analyze TCs of TS intensity or higher and ones expected to attain to TS intensity within 24 hours (ExpT) in the area, and provides the analysis information for the National Meteorological Services concerned.

Fig. 2.1 shows the flow of JMA's operation of TC analysis. Out of TCs with definite cyclonic surface wind circulation, ones with less than Beaufort Force 8 (less than 34kt) in 10-minute maximum sustained wind (MSW), Force 8 and 9 (34-47kt), Force 10 and 11 (48-63kt), and Force 12 (64kt or more) are determined as tropical depressions (TDs)<sup>4</sup>, TSs, severe tropical storms (STSs), and typhoons (TYs), respectively.

Next, TDs expected to attain to TS within 24 hours are determined as ExpTs. Furthermore, TDs except ExpTs are discriminated with respect to MSW of Force 7 (28-33kt), because JMAHQ issue marine warning for the TDs with MSW of Force 7, as well as ExpTs and TCs of TS intensity or higher. In this report, TDs with MSW of Force 7 (28-33kt) are referred to as warning-issued TD (WTD), while TDs with MSW of less than Force 7 (less than 28kt) are referred to as no-warning-issued TD (NTD).

On the other hand, TCs with lower surface pressure than surrounding area and without definite surface cyclonic wind circulation are determined as low pressure area (LPA).

In order to detect and classify TCs, JMAHQ use meteorological data such as surface observations (SYNOP, SHIP, and BUOY data), geostationary meteorological satellite images and their analysis data, QuikSCAT wind retrievals, etc. in a comprehensive manner. Among them, "satellite image analysis data" means EDA data

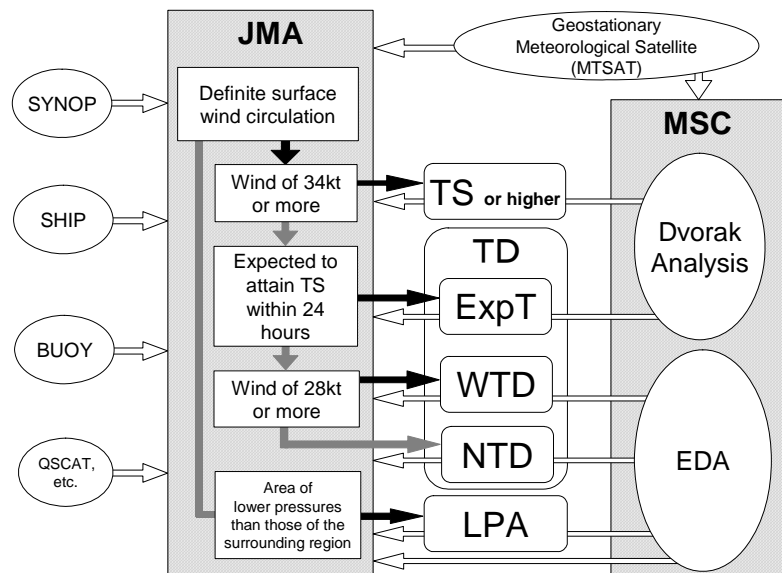


Fig. 2.1 Flow of JMA's operation of TC analysis. White arrows indicate data flow, and black and grey arrows indicate "yes" and "no", respectively.

<sup>4</sup> With respect to the formation of TDs, JMA determines TCs as TD at the first analysis of around Force 6 (22-27kt) within them.

and the Dvorak analysis data. EDA, surveyed in this study, is explained in Section 2.2.

In addition, JMAHQ post-analyze TCs which attained to TS intensity or higher during the period from the TD formation to the dissipation of TDs or transformed extratropical cyclones, combining the operational analysis data with additional data received later in order to issue Best Track data. JMAHQ also post-analyze TDs and LPAs to issue the JMA weather chart. Table 2.1 shows the items of the JMAHQ's TC analysis and the main products based on their analyses which are issued internationally.

Table 2.1 Items of TC analysis and the main products based on the analysis data which are issued internationally by JMAHQ. PS, SP, DR, CP and MSW indicate center position, speed and direction of movement, central pressure, and 10-minute maximum sustained wind, respectively.

	Items of analysis	Frequency of analysis	Main products issued Internationally
<b>Operational analysis</b>			
TS or higher	PS, SP, DR, CP, MSW, 30kt and 50kt radius	3hourly	RSMC TC advisory SafetyNET TC information
ExpT	PS, SP, DR, CP, MSW		
WTD			
NTD	PS, SP, DR, CP	6hourly	Marine warning Asia-Pacific Surface Analysis
LPA	PS, CP		
<b>Post-analysis</b>			
TS or higher	PS, SP, DR, CP, MSW, 30kt and 50kt radius	6hourly	Best track  JMA weather chart
TD before/after TS	PS, CP		
Other TD			
LPA			

**2.2 Early stage Dvorak analysis (EDA)**

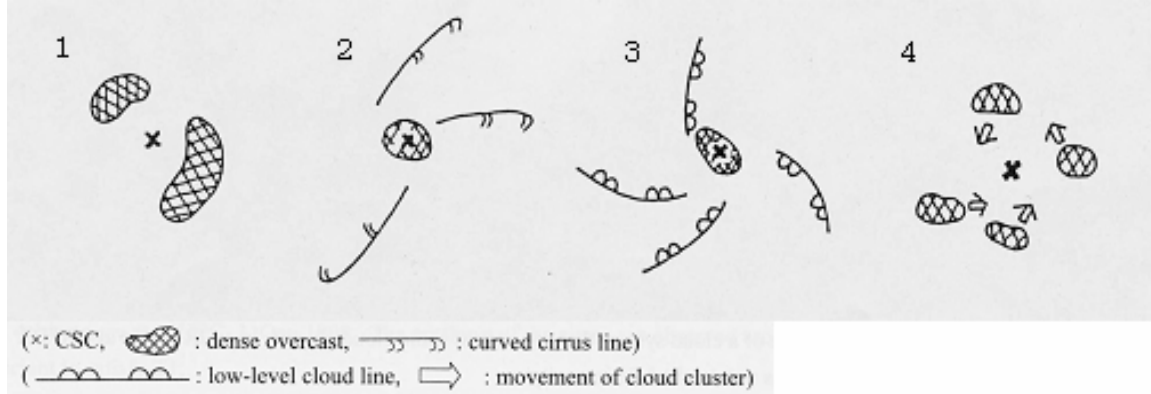
EDA consists of three steps: the detection of OCCSs, the classification of T-number 1.0 (T1.0), and the classification of T-number 1.5 and 2.0 (T1.5/2.0).

The first step of EDA is the detection of OCCSs which are convective cloud systems with a cloud system center (CSC). The CSC features proposed by Tsuchiya et al. (2000, 2001) are used in this detection. Table 2.2 shows the CSC features of Tsuchiya et al. (2000, 2001) and Dvorak (1984). In consideration of the recent improvement of satellite observation, Tsuchiya et al. (2000, 2001) supplemented the CSC features of Dvorak (1984), basically adopting them from the result of Zehr (1992) that the features of convective cloud systems developing into TSs in the western North Pacific followed them closely. Besides the 3 features of Dvorak, Tsuchiya et al. added a feature which is determined using animated satellite imagery. If a CSC can be

determined within a convective cloud system, the cloud system is regarded as an OCCS.

Table 2.2 CSC features of Tsuchiya et al. (2000, 2001) (left) and Dvorak (1984) (right). The lower figure illustrates the CSC features proposed by Tsuchiya et al.

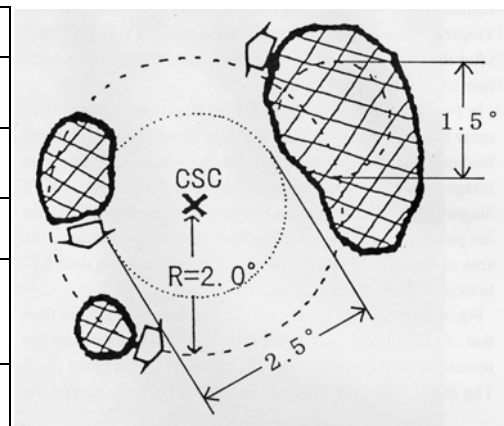
	Tsuchiya et al. (2000, 2001)	Dvorak (1984)
1	Curved band, a dense (-31°C or colder) overcast band that shows some curvature around a relatively warm (cloud minimum) area. It should curve at least one-fifth the distance around a 10° log spiral. Cirrus, when visible, will indicate anticyclonic shear across the expected CSC.	
2	Curved cirrus lines indicating a center of curvature within or near a dense, cold (-31°C or colder) overcast.	
3	Curved low cloud lines showing a center of curvature within 2° of a cold (-31°C or colder) cloud mass.	
4	Cumulonimbus clusters rotating cyclonically on animated imagery	None



As the next step of EDA, the T1.0 classification is conducted for detected OCCSs. The OCCS features proposed by Tsuchiya et al. (2000, 2001) are used in this classification. Table 2.3 shows the 5 features of OCCSs determined as T1.0, into which those of Dvorak (1984) are divided. If an OCCS satisfies all 5 features, it is determined

Table 2.3 Features of OCCSs determined as T1.0. The right figure illustrates an OCCS determined as T1.0.

	Tsuchiya et al. (2000, 2001)
1	A convective cloud system has persisted for 12 hours or more.
2	The cloud system has a CSC defined within a diameter of 2.5° latitude or less.
3	The CSC persists for 6 hours or more.
4	The cloud system has an area of dense, cold (-31°C or colder) that appears less than 2° latitude from the center.
5	The above overcast is more than 1.5° latitude in diameter.



as T1.0. Otherwise it is determined as the T-number of less than 1.0.

For OCCSs determined as T1.0 consecutively, the T1.5/2.0 classification is conducted. Regarding this classification, MSC supplemented the method of Dvorak (1984), which had no detailed description about it, with some rules. In this classification, an OCCS is observed with respect to the time variation in the organization such as the curvature and length of convective curved bands and the cyclonical rotation of convective cloud areas. If it is determined to be more organized than at the previous analysis, 0.5 is added to the previous T-number. If it is determined to be less organized, 0.5 is subtracted from the previous T-number, considering the T-number not to be less than 1.0. It is to be noted that this classification is conducted referring the PT chart of Dvorak (1984) to ensure the continuity to the Dvorak analysis. The contents and an example of EDA are shown in Table 2.4 and Fig. 2.2, respectively.

Table 2.4 Contents of EDA

Frequency	6hourly (00, 06, 12, 18UTC)	
Procedure	1. OCCS detection	Dvorak (1984) supplemented by Tsuchiya et al. (2000, 2001)
	2. T1.0 classification	
	3. T1.5/2.0 classification	Dvorak (1984) supplemented by MSC
Contents	CSC position, T-number	

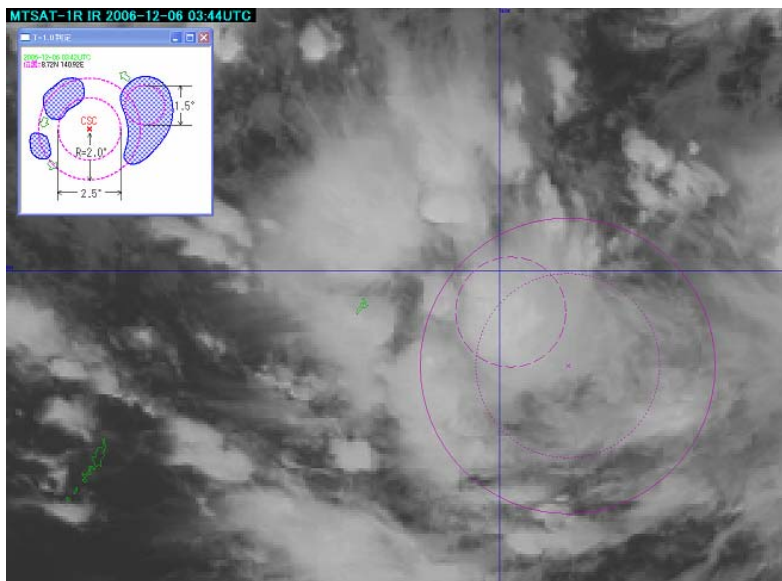


Fig. 2.2 Screen capture of EDA for a tropical disturbance over the sea east of Yap Island at 04UTC on 6 December 2006

### 3. Verifications and discussions

In this section, OCCSs detected through EDA are compared with TCs on weather charts to verify the following issues:

- Correspondence of OCCSs to TCs (Section 3.2)
- Development of OCCSs into TCs (Section 3.3)
- Timing of the detection of OCCSs and the development of TCs (Section 3.4)

### 3.1 Preparation for the verifications

#### *Classification of TCs*

Table 3.1 describes the classification of TCs used for the verifications.

Table 3.1 Classification of TCs

Grade	
LPA	TCs without definite cyclonic surface wind circulation where surface air pressure are lower than those of the surrounding
NTD	TCs with definite cyclonic surface wind circulation and MSW of Beaufort scale of less than Force 7 (less than 28kt)
WTD	TCs with definite cyclonic surface wind circulation and MSW of Force 7 (28-33kt)
TS	TCs with definite cyclonic surface wind circulation and MSW of Force 8 and 9 (34-47kt)

#### *Data used for the verifications*

The 5-year data of OCCSs and TCs (NTDs, WTDs, and LPAs) from 2002 to 2006 are used for the verifications due to the homogeneity of OCCS data<sup>5</sup>. Operational analysis data are used for OCCSs, NTDs, WTDs, and LPAs, while post-analysis data for TSs. The followings are reasons why operational analysis data are used except for TSs:

- OCCS data are not post-analyzed.
- TDs are classified into NTDs and WTDs only in the operational analysis.
- Post-analysis data of LPAs are not archived in digital format.

#### *Matching of OCCSs with TCs*

In order to compare OCCSs with TCs on weather charts, a definition needs to be established for their matching. In these verifications, it is defined that an OCCS corresponds to a TC when the center position of the TC is within about 4° in latitude and longitude from the CSC. The basic concept of this definition is that an OCCS corresponds to a TC whose center position is within the domain of the OCCS. The domain is, in the verifications, limited to the area within about 4° in latitude and longitude from CSC, where primary convective cloud area forming an OCCS is seen using the 4<sup>th</sup> and the 5<sup>th</sup> features in Table 2.3.

#### *Definition of base time points*

Base time points are defined as described in Table 3.2. The numbers of OCCSs which reached each time point from 2002 to 2006 are also shown in the same Table.

---

<sup>5</sup> Terasaka et al. (2007) reported that OCCS data have a gap between ones before and after 2002 due to the minor change of the EDA procedure in the year.

Table 3.2 Definition of base time points and the numbers of OCCSs which reached each time point

Base time point		Number of OCCSs
FDOCS	First detection of an OCCS	453
FDT10	First determination of an OCCS as T1.0	188
FDT15	First determination of an OCCS as T1.5	112 <sup>6</sup>
FDT20	First determination of an OCCS as T2.0	41 <sup>6</sup>
FDTs	First determination of an OCCS as TS	119

### 3.2 Correspondence of OCCSs to TCs

Fig. 3.1 shows the total numbers<sup>7</sup> analyzed as TCs on weather charts which had an OCCS detected through EDA from 2002 to 2006. Out of the total 2589, 809 and 512 analyses<sup>8</sup> of LPAs, NTDs and WTDs on weather charts, 587 (23%<sup>8</sup>), 611 (75%<sup>8</sup>) and 497 (97%<sup>8</sup>) analyses corresponded to OCCSs, respectively. These results reveal that many of NTDs and WTDs corresponded to OCCSs, while many of LPAs did not. Hereinafter, OCCS data are not verified for LPAs.

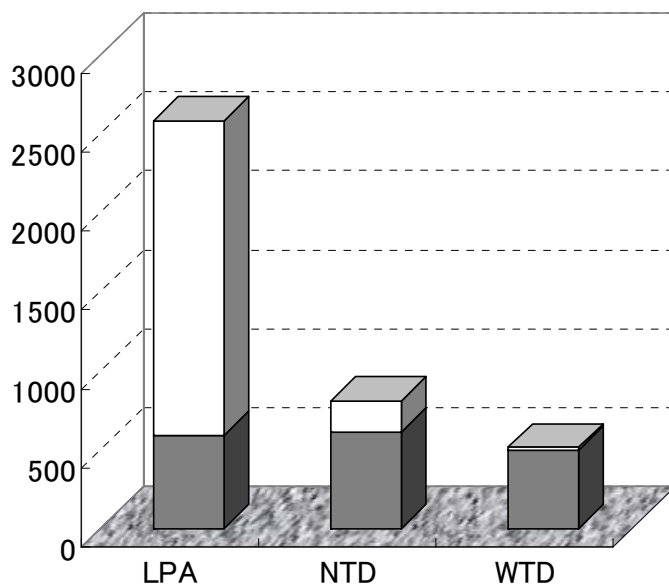


Fig. 3.1 Total number of analyses of TCs on weather charts with OCCSs (grey bars) and without OCCSs (white bars)

<sup>6</sup> Numbers of FDT15- and FDT20-reached OCCSs were less than that of FDTs-reached, because many OCCSs were determined as ExpT, for which EDA was terminated, before they reached FDT15.

<sup>7</sup> The analysis number of a TC and the detection number of an OCCS are counted for every analysis and detection in weather map analysis conducted four times a day (00, 06, 12 and 18UTC).

<sup>8</sup> These total analyses include those of weakening TCs, such as ones located over land, many of which did not have an OCCS. Therefore, the percentages of TCs only in early developing stage with an OCCS should be higher to some extent than those in this sentence.

### 3.3 Development of OCCSs into TCs

Fig. 3.2 shows the percentages of OCCSs which finally attained to NTD, WTD and TS out of all ones which reached each time point as follows:

- Out of all FDOCS-reached OCCSs, 47%, 34% and 26% finally attained to NTD, WTD, and TS, respectively.
- Out of all FDT10-reached ones, 89%, 78% and 61% attained.
- Out of all FDT15-reached ones, 97%, 95% and 79% attained.
- Out of all FDT20-reached ones, 100%, 100% and 98% attained.

They reveal the percentage of OCCSs which finally attained to TS was low before FDT10, while high at or after FDT10.

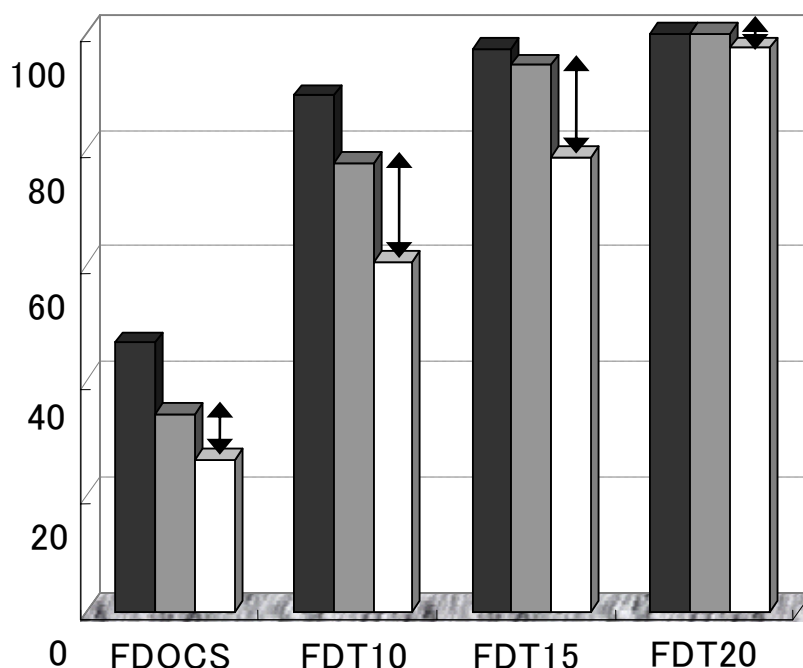


Fig. 3.2 Percentage (%) of OCCSs which finally attained to NTD (dark grey bars), WTD (light grey bars) and TS (white bars) out of all ones which reached each time point. Arrows indicate the percentages of ones which finally attained to WTD not TS.

### Discussion

This figure also shows that, with respect to the percentage of OCCSs which finally attained to WTD not TS, the percentages of FDT10- and FDT15-reached ones were higher than those of FDOCS- and FDT20-reached.

This result is firstly discussed by comparing the tracks of TS-attained and not-TS-attained OCCSs out of FDT10-reached ones (Figure 3.3). This figure reveals that many of not-TS-attained ones were located over the sea around the Philippines or in the South China Sea at FDT10, and then dissipated on or near land. Secondly, the percentages of TS-attained ones are compared between two groups: the group of OCCSs located to the west of 130°E (130W-OCCSs), relatively close to land area, at each time

point, and the other group of ones located to the east of 130°E (130E-OCCSs), relatively far from land area (Fig. 3.4).

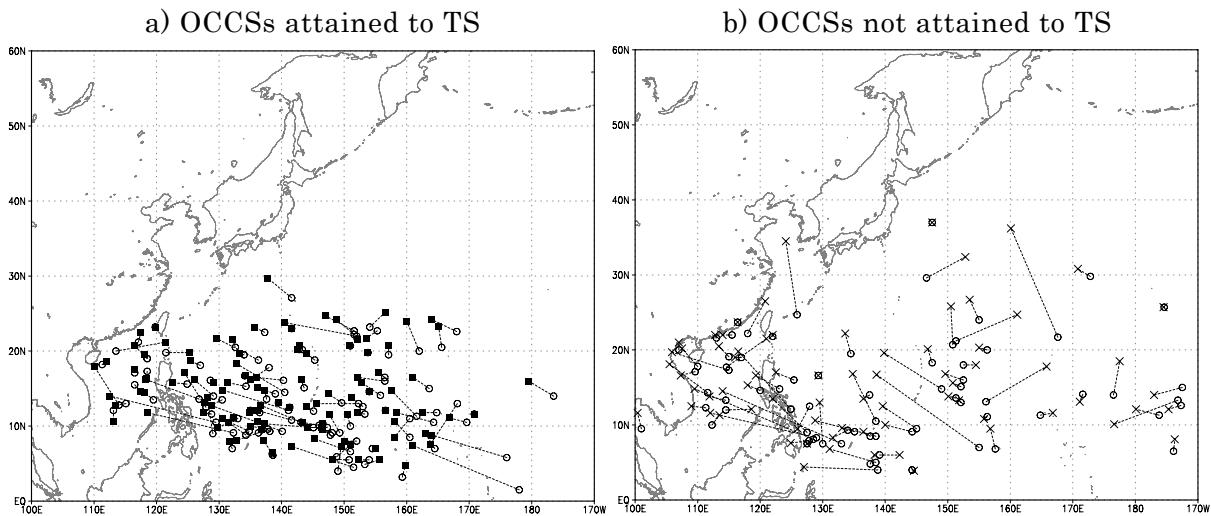


Fig. 3.3 Tracks of FDT10-reached OCCSs which finally attained to a) TS and b) not TS. Open circles, squares and crosses indicate the positions at FDT10, the determination as ExPT (the termination of EDA) and the dissipation, respectively.

The results are as follows:

- Regarding FDT10- and FDT15-reached OCCSs, 43% and 59% of 130W-OCCSs and 67% and 86% of 130E-OCCSs finally attained to TS, respectively. The differences between the two groups were relatively large (about 25%).
- Regarding FDOCS- and FDT20-reached OCCSs, 17% and 92% of 130W-OCCSs and 29% and 100% of 130E-OCCSs finally attained to TS, respectively. The differences between the two groups were relatively small (about 10%).

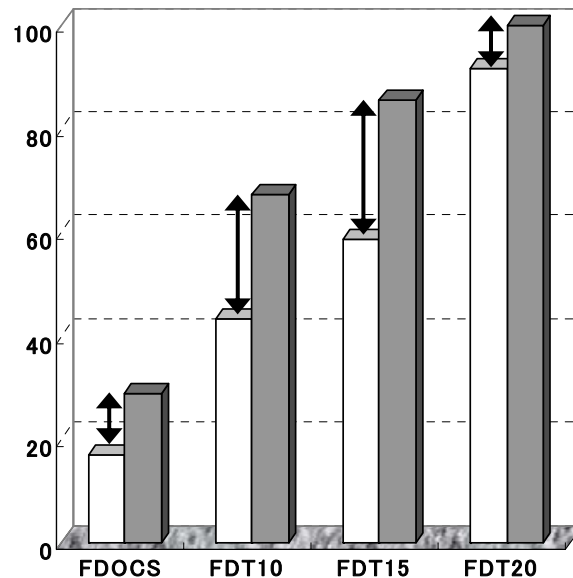


Fig. 3.4 Percentage (%) of OCCSs at each time point which finally attained to TS

White and grey bars indicate the percentages of 130W-, 130E-OCCSs, respectively. Arrows indicate the differences between those of 130W- and 130E-OCCSs.

The above comparative results reveal that it was a key factor to attain to TS for OCCSs especially at FDT10 or FDT15 to "be located far from land area".

### 3.4 Timing of the detection of OCCSs and the development of TCs

Fig. 3.5 shows the percentages of NTD- and WTD-attained OCCSs before, at, and after each time point. The results are as follows:

- 6% and 1% of FDOCS-reached OCCSs attained to NTD and WTD before FDOCS, respectively.
- 12% and 2% of FDOCS-reached OCCSs attained to NTD and WTD at FDOCS.
- 74% of FDT10-reached OCCSs attained to NTD before or at FDT10.
- 80% of FDT15-reached OCCSs attained to WTD before or at FDT15.
- 97% of FDT20-reached OCCSs attained to WTD before or at FDT20.

They reveal that many of FDT10-reached ones attained to NTD before and at FDT10, and many of FDT15-reached ones attained to WTD before or at FDT15.

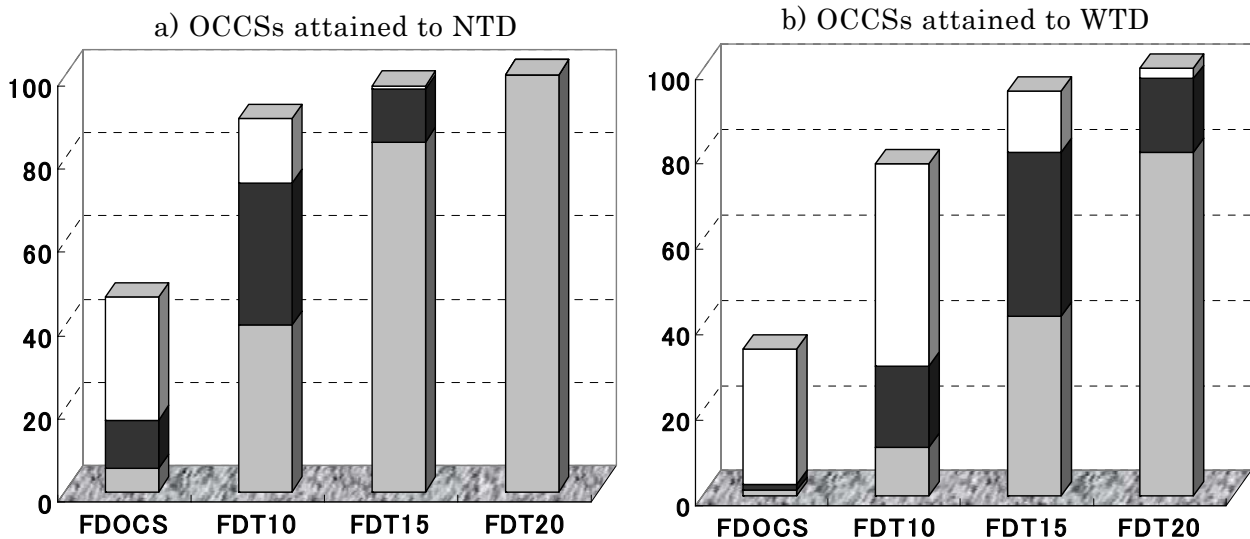


Fig. 3.5 Percentage (%) of OCCSs which attained to a) NTD and b) WTD before (light grey bars), at (dark grey bars), and after (white bars) each time point, respectively

Fig. 3.6 shows the average period from each time point (FDOCS, FDT10, FDT15, and FDT20) to FDTS: 2.3, 1.4, 0.8 and 0.4 days. This result agrees well with the model for the development of TCs shown by Dvorak (1984), and reveals that EDA is appropriate for analysis based on Dvorak.

### Discussion

In the process of this verification, it was found that 2 out of 119 TS-attained OCCSs from 2002 to 2006 were determined as ExpT before FDT10, and their positions at FDOCS were 19°N and 29°N, both in relatively high latitudes.

Therefore, the average period from each time point to FDTS is examined for three groups of OCCSs depending on latitude: the group of ones located to the south of  $10^{\circ}\text{N}$  at each time point (S-OCCSs), the group of ones located from  $10^{\circ}\text{N}$  to  $20^{\circ}\text{N}$  (M-OCCSs), and the group of ones located to the north of  $20^{\circ}\text{N}$  (N-OCCSs). In this regard, no OCCSs attained to TS which were located to the north of  $30^{\circ}\text{N}$  at each time point. The results are shown in Fig. 3.7 as follows:

- The average period from each time point (FDOCS, FDT10 and FDT15) to FDTS was 2.8, 1.9 and 1.2 days for S-OCCSs, while 1.7, 1.2 and 0.6 days for N-OCCSs, respectively. In particular, the average period from FDOCS to FDTS for N-OCCSs was about one day shorter than for S-OCCSs.
- Regarding the average period from FDT20 to FDTS, difference depending on latitude was relatively small.

These results reveal that OCCSs located in higher latitude, except FDT20-reached ones, had a tendency to develop to TS in a shorter time.

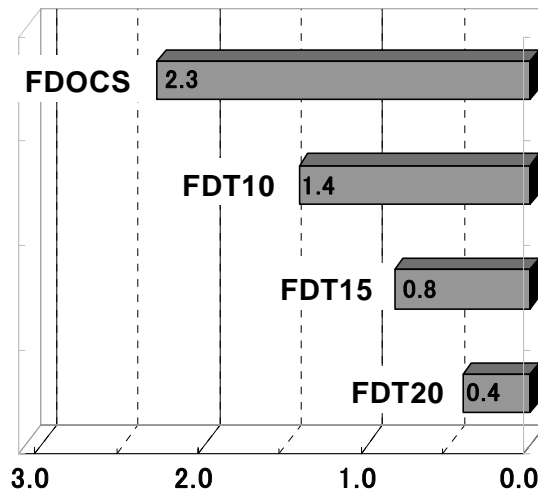


Fig. 3.6 Average period (days) from each time point to FDTS

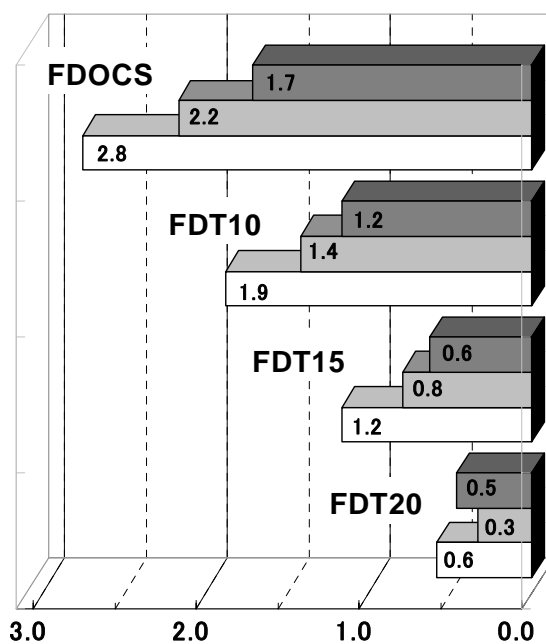


Fig. 3.7 Average period (days) from each time point to FDTS depending on latitude. White, light grey and dark grey bars indicate average periods for S-, M- and N-OCCSs, respectively.

#### 4. Summary of the study

The results of the study are summarized in Table 4.1. OCCSs can be acknowledged as follows from the verification results:

- NTDs and WTDs usually have an OCCS, while LPAs do not.
- OCCSs determined as the T-number of less than 1.0 have considerable possibility to attain to NTD. On the other hand, few OCCSs attain to NTD before FDOCS. They attain to TS in about 2.5 days after FDOCS on the condition that they develop steadily.
- OCCSs determined as the T-number of 1.0 have very high possibility to attain to WTD, and have high possibility to attain to TS. They usually attain to NTD before or at FDT10. They attain to TS in about 1.5 days after FDT10 on the condition that they develop steadily.
- OCCSs determined as the T-number of 1.5 have very high possibility to attain to TS. They usually attain to WTD before or at FDT15. They attain to TS in about 1.0 days after FDT15 on the condition that they develop steadily.
- Most of OCCSs determined as the T-number of 2.0 attain to TS. They attain to TS in about 0.5 days after FDT20.

In addition, the followings should be noted from the results of discussions:

- OCCSs expected not to approach to land area, especially at FDT10 or FDT15, have higher possibility to attain to TS.
- OCCSs located in higher latitudes tend to attain to TS in a shorter time.

Table 4.1 Results of the study (from 2002 to 2006). Numbers in parenthesis indicate the results for OCCSs which were located to the east of 130° E at each base time point.

Base time point (BTP)	Number of OCCSs reached each BTP	Percentage (%) of OCCSs attained NTD and WTD before or at each BTP		Percentage (%) of OCCSs which finally attained to NTD, WTD and TS			Average period (days) from each BTP to FDTS
		NTD	WTD	NTD	WTD	TS	
FDOCS	453 (346)	17	3	46	34	26 (29)	2.3
FDT10	188 (135)	74	30	89	78	61 (67)	1.4
FDT15	112 (83)	96	80	97	95	79 (86)	0.8
FDT20	41 (29)	100	97	100	100	98 (100)	0.4

## References

- K. Bessho, T. Nakazawa, S. Nishimura, K. Kato, and S. Hoshino (2006): Statistical analysis of organized cloud clusters on western North Pacific and their warm core structure, 27<sup>th</sup> Conference on Hurricanes and Tropical Meteorology, April 24-28, Monterey, CA.
- Dvorak, V.F. (1984): Tropical Cyclone Intensity Analysis Using Satellite Data, NOAA Technical Report NESDIS 11, U.S. Dept. of Commerce.
- Y. Terasaka, T. Nakanishi and S. Nishimura (2007): The accuracy of "Discriminating method of cloud systems which develop into tropical cyclone in the early stage" and the lead times to becoming the typhoon, Meteorological Satellite Center Technical Note No. 48 (in print).
- A. Tsuchiya, T. Mikawa and A. Kikuchi (2000): Discriminating method of cloud systems which develop into tropical cyclone in the early stage, Meteorological Satellite Center Technical Note No. 38, 13-19 (in Japanese).
- Tsuchiya, A., Mikawa, T. and Kikuchi, A. (2001): Method of Distinguishing between Early Stage Cloud Systems that Develop into Tropical Storms and Ones that Do Not, Geophysical Magazine Series 2, Vol.4, Nos.1-4, 49-59.
- T. Ueno (2002): Application of "Discriminating method of cloud systems which develop into tropical cyclone in the early stage" to the period in 2000 and 2001 and Environment of the cloud systems which develop into tropical cyclone in the South China Sea, Meteorological Satellite Center Technical Note No.41, 1-14 (in Japanese).
- World Meteorological Organization (2005): Typhoon Committee Operational Manual – Meteorological Component, WMO/TD-No.196, World Meteorological Organization.
- Zehr, R.M. (1992): Tropical Cyclogenesis In the Western North Pacific, NOAA Technical Report NESDIS 61, U.S. Dept. of Commerce.